 CMC, vol.48, no.1, pp.1-23, 2015

Minimizing Thermal Residual Stress in Ni/Al_2O_3 Functionally Graded Material Plate by Volume Fraction Optimization

Xing Wei[1,2], **Wen Chen**[1,3], **Bin Chen**[1]

Abstract: The thermal residual stress in the fabrication of functionally graded material (FGM) systems can give rise to various mechanical failures. For a FGM system under a given fabrication environment, the thermal residual stresses are determined by the spatial distribution of its constituent components. In this study, we optimize a Ni/Al_2O_3 FGM plate aiming at minimizing the thermal residual stresses through controlling its compositional distribution. Material properties are graded in the thickness direction following a power law distribution in terms of the volume fractions of constituents (P-FGM). An analytical model and a hybrid genetic algorithm with the pattern search are employed to predict and to minimize the thermal residual stresses, respectively. Simulation results show that an optimal design of the FGM plate could help fulfill its potential in reducing the thermal residual stresses.

Keywords: Functionally graded material; Ni/Al_2O_3; Composition optimization; Thermal residual stresses; Hybrid genetic algorithm.

1 Introduction

Nowadays, ceramic/metal composite materials are widely used in various engineering fields. Due to the poor mechanical property compatibility of different materials, the thermal residual stress is induced in the manufacturing process and is a potential risk leading to the mechanical failures in the long-term service of the composites. A heat-resistant material, dated back to 1984 during a space plane project in Japan

[1] State Key Laboratory of Hydrology-Water Resources and Hydraulic Engineering & Center for Numerical Simulation Software in Engineering and Sciences, College of Mechanics and Materials, Hohai University, Nanjing, Jiangsu, 210098, China

[2] College of Civil Engineering and Architecture East China Jiaotong University, Nanchang 330013, China

[3] Corresponding author, Tel.: +86 25 83786873; fax: +86 25 83736860. E-mail address: chenwen@hhu.edu.cn

[Lee, Stinton, Berndt, Erdogan, Lee, and Mutasim (1996)], offers a solution to reduce the thermal stresses [Nemat-Alla (2003)], which is nowadays well-known as functionally graded/gradient material (FGM).

The FGM is characterized by gradually spatial variation in volumetric fractions of two or more constituent phases, which integrates desirable physical properties of different components. Owing to its superior mechanical performances, the FGMs have been applied in many fields [Koizumi (1997); Attia, Meguid, and Nouraei (2012)]. It is worthy of noting that the FGM permits tailoring of its microstructure, which determines its mechanical performances under given loads and environments. An optimal design may derive maximal benefits from a FGM system in terms of particular application requirements. Elishakoff (2012) determined the variation of the elastic modulus along the axial coordinate to achieve a predesigned buckling mode under given loading and boundary conditions. Goupee and Vel [Goupee and Vel (2006)] optimized the natural frequencies of functionally graded structures by tailoring their material distribution. Optimal designs of the FGM dental implant have also been developed to advance osseointegration and bone remodeling [Lin, Li, Li, Zhou, and Swain (2009); Hedia and Mahmoud (2004)].

Since thermal analysis is a crucial issue in a wide variety of the FGM applications, the optimal FGM design for thermal stress reduction has attracted great attention. Markworth and Saunders (1995) developed a simplified model to optimize the FGM, in which the volume fraction of metal was assumed to be described by a specific functional form. Tanaka, Watanabe, Sugano, and Poterasu (1996) tailored a hollow cylinder and globally reduced the thermal stresses in the FGM by means of the incremental finite element method. Cho and Ha (2002) minimized steady-state thermal stresses in Ni/Al_2O_3 heat-resisting FGM composites with interior penalty-function method and golden section method. Yoshihiro Ootao (2000) took the functionally graded plate as a laminated composite plate, and optimized its material composition in each layer for thermal stress reduction with a genetic algorithm.

But nevertheless few of the above-mentioned studies are concerned with the thermal residual stresses, which are associated with many mechanical failures of composite materials [Qian, Nakamura, and Berndt (1998)]. Because of its vital importance, this study aims at minimizing the thermal residual stresses by designing an optimum Ni/Al_2O_3 FGM plate with a power law distribution of the volume of constituents. The thermal residual stresses are calculated by Ravichandran's model [Ravichandran (1995)], which was reported in good agreement with the FEM [Sahay and Ravichandran (1996)] for a Ni/Al_2O_3 FGM system. The material composition distribution is optimized by a hybrid genetic algorithm with the pattern search (GA-PS). We identify promising areas of the search space with the genet-

ic algorithm (GA), and improve approximations to the minimum with the pattern search (PS). Numerical results show that an optimal composition distribution of a FGM system can dramatically reduce the thermal residual stresses.

The rest of the paper is organized as follows. In Section 2, an analytical model of the thermal residual stress in the FGM system is introduced. The formulation of the optimization is presented and addressed with the GA-PS in Section 3. Section 4 tests the numerical feasibility and efficiency of the proposed method to four benchmark cases, including the single- and multi-objective optimizations. Finally, some concluding remarks are summarized in Section 5.

2 Analytical model of the thermal residual stress

An accurate and effective prediction model of thermal residual stress is essential for the optimization of the FGM microstructure. In this section, the material distribution model, effective property estimation and the analytical model are set up for the optimization.

2.1 Material model

Fig. 1 gives a schematic description of a FGM plate of thickness h. The plate is fully ceramic at the bottom layer and fully metal at the top layer. The ceramic-metal joint region continuously varies from ceramic to metal though the thickness (z-axis). The distribution of the material in functionally graded structures may be designed to various spatial specifications, including polynomial distribution [Mark-

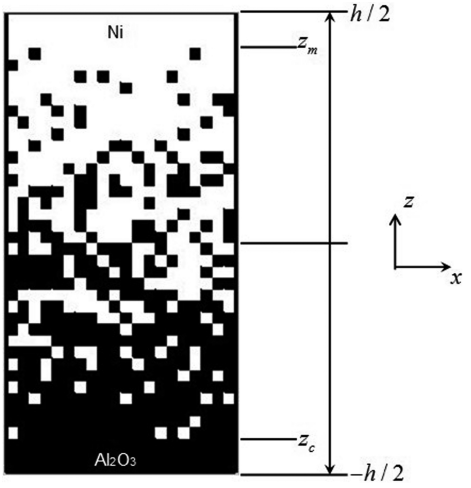

Figure 1: Schematic description of a FGM system.

worth and Saunders (1995)], power law distribution [Reddy (2000)], piecewise spline interpolation [Goupee and Vel (2007); Taheri, Hassani, and Moghaddam (2014)], etc. This paper investigates the power-law distribution (P-FGM), and the volume fractions of metal and ceramic, V_m and V_c, are assumed as

$$V_c(z) = \begin{cases} 1, & -h/2 \le z \le z_c \\ \left[\dfrac{z_m - z}{z_m - z_c}\right]^N, & z_c \le z \le z_m \\ 0, & z_m \le z \le h/2 \end{cases}, \quad V_m = 1 - V_c, \tag{1}$$

where z_c and z_m are coordinates of interface between the ceramic layer and FGM layer, and the FGM layer and metal layer, N is the exponent of the power law function in the graded region. Accordingly, the effective physical properties of the FGM layer can be estimated with regard to the volume variation. The total thickness of the plate, h, is 0.01 m, and the material properties of the constituents are given in Tab. 1.

Table 1: Material properties for Ni and Al_2O_3.

Material property	Ni	Al_2O_3
E (GPa)	199.5	393.0
v	0.3	0.25
α (1e-6/K)	15.4	7.4
ρ (kg/m^3)	8880	3960

The effective modulus of elasticity in the graded region is determined as

$$E = \frac{(E_m E_c - E_m^2)(1 - V_c^{1/3} + V_c) + E_m^2}{E_c + (E_m - E_c)V_c^{1/3}}, \tag{2}$$

where E_m and E_c refer to elastic modulus of metal and ceramic, respectively. This model is proposed by Ravichandran, and it is reported that this Young's modulus well coincides with experimental data [Ravichandran (1994)].

For the volume-averaged thermal expansion coefficients, Cho observed Schapery's estimation on the thermal expansion coefficients leads to the most adequate thermal stress distributions in his numerical experiments [Cho and Ha (2001)]. Schapery's estimation is therefore employed to evaluate the volume-averaged thermal expansion coefficients as

$$\alpha = V_m \alpha_m + V_c \alpha_c - \frac{\Lambda - 1/\bar{K}}{1/K_m - 1/K_c}(\alpha_m - \alpha_c), \tag{3}$$

where

$$\bar{K} = V_m K_m + V_c K_c$$
$$\Lambda = \frac{V_m}{K_m} + \frac{V_c}{K_c} \quad .$$

2.2 Analytical model

Considerable works, including both numerical methods [Chen and Jie (2007); Delfosse, Cherradi, and Ilschner (1997); Fukui and Watanabe (1996); Wang and Qin (2008); Dong, El-Gizawy, Juhany, and Atluri (2014); Dong, El-Gizawy, Juhany and Atluri (2014)] and analytical methods [Ravichandran (1995); Zhang, Xu, Wang, Jiang, and Wu (2006); Shaw (1998); Becker Jr, Cannon, and Ritchie (2000)], have been devoted to investigating the thermal residual stresses in the FGM system. If applicable, the analytical methods allow a quicker and easier evaluation on the thermal residual stresses. Ravichandran proposed an analytical model [Ravichandran (1995)] to calculate the thermal residual stress in the ceramic/metal joint FGM system. Furthermore, he demonstrated the analytical results are in good agreement with the FEM results [Sahay and Ravichandran (1996)] for Ni/Al_2O_3 FGM plates. Bouchafa, Benzair, Tounsi, Draiche, Mechab, Adda Bedia (2010) used this model to evaluate the thermal residual stresses in the FGM with material properties varying exponentially through the thickness (E-FGM). Buoyed by the great success of this model, it is adopted to evoluate the thermal residual stress.

In Ravichandran's model [Ravichandran (1995)] (Fig. 2), two principal parts are involved in the thermal residual stress, one arising from stress equilibrium due to contraction or expansion, and the other from moment equilibrium due to the asymmetric stress distribution.

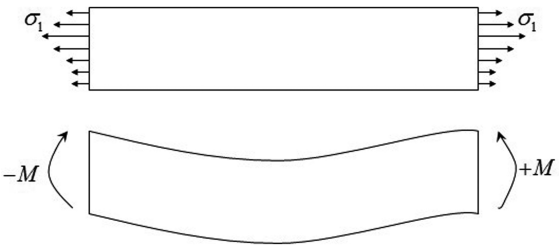

Figure 2: Mechanical analysis on the FGM system.

The first part of the thermal residual stresses is caused after the FGM plate cools down from high processing temperature. The residual stress is developed due to

the constrains in the x direction at two ends, and its magnitude is

$$\sigma_{r1}(z) = \alpha(z)E(z)\Delta T - E(z)\frac{\int_{-h/2}^{h/2}\alpha(z)E(z)\Delta T dz}{\int_{-h/2}^{h/2}E(z)dz}. \tag{4}$$

The second part of the residual stress is caused by the removal of the constraints which prevent the bending of the FGM plate would be relaxed, and the stress distribution is therefore rearranged. The additional stress arising from the bending of the plate is given as

$$\sigma_{r2}(z) = ME(z)\frac{z\int_{-h/2}^{h/2}E(z)dz - \int_{-h/2}^{h/2}E(z)zdz}{\int_{-h/2}^{h/2}E(z)dz\int_{-h/2}^{h/2}E(z)z^2dz - \left[\int_{-h/2}^{h/2}E(z)zdz\right]^2}. \tag{5}$$

The total residual stress in the FGM in absence of constraints is obtaining by adding Eqs. (4) and (5) as

$$\sigma_r(z) = E(z)\Delta T\left[\alpha(z) - \frac{A_1}{E_1} - \frac{(A_2 - \frac{A_1}{E_1}E_2)(zE_1 - E_2)}{E_1E_3 - E_2^2}\right], \tag{6}$$

where

$$\begin{aligned}(A_1, A_2) &= \int_{-h/2}^{h/2}(1,z)\alpha(z)E(z)dz \\ (E_1, E_2, E_3) &= \int_{-h/2}^{h/2}(1,z,z^2)E(z)dz\end{aligned}. \tag{7}$$

In this paper, the processing temperature T_f and room temperature T_0 are assumed to be 1373 K and 298 K, respectively. Consequently, the temperature difference ΔT is 1075 K for the following computations. It should be noted that Eq. (6) is solid when the bending of the FGM plate is prevented by the constraints.

3 Composition optimization for FGMs

In this section, the optimization of the compositional distribution is formulated to minimize the thermal residual stresses and mass for the FGM systems. For the multi-objective optimization, the weighted sum method is employed to combine all objective functions into a single function. And then the optimization problems are solved by a hybrid genetic algorithm with the pattern search.

3.1 Formulation of the optimization problem

Since material properties are graded in the thickness direction according to a power law distribution in terms of the volume fractions of constituents as (1), the optimization of the material distribution is simplified to choose an optimal volume fraction exponent, N, and the thicknesses of the ceramic and metal substrates t_c, t_m. As a result, the constrained optimization problem is described as

$$\begin{array}{ll} \text{Find} & N, t_c, t_m \\ \text{Minimize} & \mathbf{f}(N,t_c,t_m) = [f_1(N,t_c,t_m), f_2(N,t_c,t_m), \ldots, f_k(N,t_c,t_m)] \\ & k = 1,2,\cdots \\ \text{Subject to} & g_j(N,t_c,t_m) \le 0, \;\; j = 1,2,\cdots \\ & 0.01 \le N \le 100 \end{array} \tag{8}$$

where $f_k(N,t_c,t_m)$ is the kth objective function to be minimized, $g_j(N,t_c,t_m)$ is the constraint function in the optimization. When N is close to 0 or infinite, the material tends to pure ceramic or metal. Therefore, the design variable, N, is bounded by 0.01 and 100.

If more than one objective functions are involved in the optimization, namely, multi-objective optimization problem [Marler and Arora (2004); Deb (2001)], the weighted sum method is used to transform the multi-objective optimization problem into a single composite objective function

$$f(N,t_c,t_m) = \sum_{i=1}^{k} \omega_i f_i(N,t_c,t_m), \tag{9}$$

where $\{\omega_i\}$ is a vector of weights set by the decision-maker, and $\sum_{i=1}^{k} \omega_i = 1$, and $\omega_i > 0$. In general, the value of the weight is proportional to the relative importance of the objective functions. For the sake of the difference among objective functions, it is advantageous to transform the original functions into a consistent form. Therefore, we normalize the objective functions as

$$f_i^{trans} = \frac{f_i(N,t_c,t_m) - f_i^{\min}}{f_i^{\max} - f_i^{\min}}, \tag{10}$$

where $f_i^{\max}$, $f_i^{\min}$ are the minimal and maximal value in design as the normalized values. Some of papers also suggest that the nadir and ideal objective value would be used as normalized values. Then, the unified objective function can be recast as

$$f(N,t_c,t_m) = \sum_{i=1}^{k} \omega_i f_i^{trans}(N,t_c,t_m). \tag{11}$$

3.2 Hybrid genetic algorithm with pattern search

Genetic algorithms (GAs) [Deb (2001)] are a category of search and optimization methods that imitates the evolution of a creature and is based on the mechanism of natural genetics. A GA begins its search with a population of randomly generated individuals, and then the next generation is produced by selection, crossover, and mutation. The fitness of every individual in the population is evaluated in each generation. In the optimization, the fitness function is the objective function. Finally, the algorithm terminates when either a maximal number of generations or a satisfactory convergence has been achieved.

Although the GAs can rapidly locate the promising region in which the global optimum exists, they converge slowly to the best solution in the explored region due to its inability to make small moves in the neighborhood of current solutions. As a consequence, a local research approach is resorted to find a better solution in promising region guided by the GA. We consider the pattern search (PS) [Audet and Dennis (2002)] to fine-tune the approximations. The pattern search chooses a certain set of search directions at each iteration and evaluates the objective function at a given step length along each of these directions. The PS updates the estimate to the best of the sampled solutions in the current iteration, and refines the mesh for the next iteration.

In this study, an optimal solution is generated by the GA, and then fed to the PS algorithm for a fine-tuning approximation. For the GA, the size of the initial population is 100, and the maximal number of generations is 10, 80% of the population in each generation is subjected to uniform crossover. The adaptive feasible mutation [Srinivas and Patnaik (1994)] is employed in this study. This method adds a randomly generated number to each element in the child population. The direction of the random number is adaptive to the last successful or unsuccessful generation, the relative constraints and inequality constraints. The PS is set to be terminated when $\Delta_k < 10^{-6}$. The procedure of the hybrid method, GA-PS, is shown in flowchart in Fig. 3. We implement the GA and PS using the Matlab Global Optimization Toolbox software V 3.2.

4 Numerical results and discussions

In this section, the optimization of the FGM is presented via the GA-PS. Firstly the impact of the parameters, *viz* the exponent and thicknesses of the substrates, is analyzed. Subsequently, the ceramic volume fraction is optimized to minimize the maximal thermal residual stresses in the second case. In the third case, the optimization of the thicknesses of the substrates is also taken into account for the thermal residual stress minimization. In the fourth case, we solve a multi-objective

optimization problem concerning the thermal residual stress and mass.

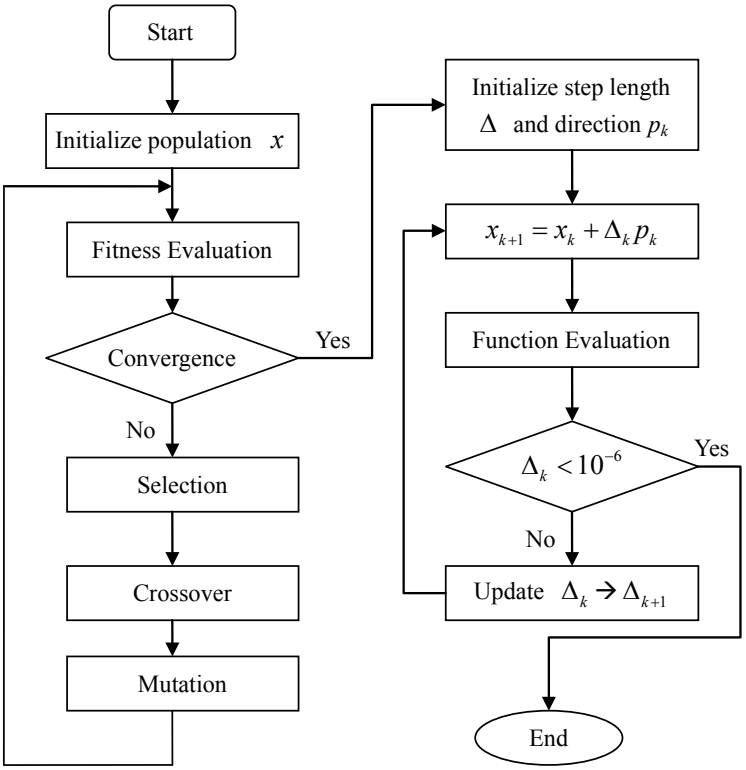

Figure 3: Flowchart for hybrid GA-PS.

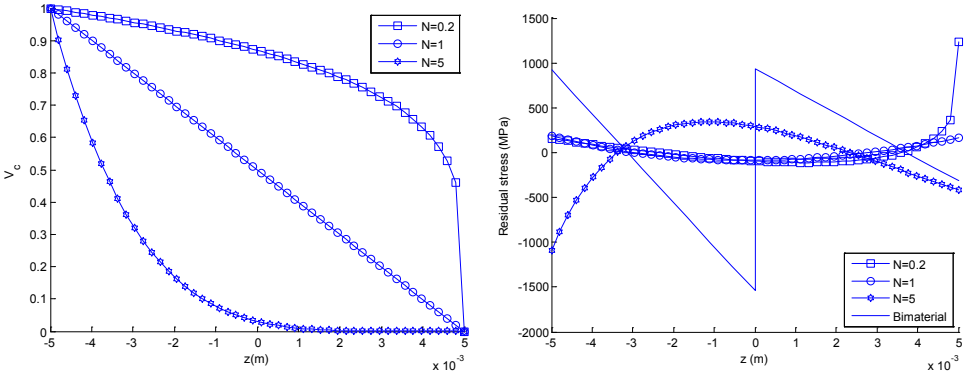

(a) (b)

Figure 4: Volume fraction distribution (a) and thermal residual stresses (b) in the FGM system without.

4.1 Thermal residual stress analysis

This section investigates how the volume fraction impacts the distribution of the thermal residual stresses by using graded microstructure with varying exponents and thicknesses of the substrates.

Fig. 4 displays the results of the FGM systems without substrates. The thermal residual stresses of the non-graded bimaterial are also depicted for a comparison. The maximal tensile, $\sigma_{t\max}^{bi}$, and compressive stresses, $\sigma_{c\max}^{bi}$, in the non-graded system are 933.98 MPa and 1540.0 MPa respectively. In stark contrast with the non-graded material, a reduction more than 90% of the maximal thermal residual stresses can be observed when $N = 1$. The results of $N = 0.2$ are similar to that of $N = 1$, but obtain larger tensile stress in the metal-rich region than that in the non-graded system. The reduction of the maximal thermal residual stresses for $N = 5$ is not so significant, but nevertheless more than 30% can be achieved.

In Fig. 5–Fig. 6, different sizes (5%, 25% of plate thickness) of the metal and ceramic substrates are taken into account. Linear behavior of the thermal residual stresses can be observed in the substrates. It is manifested that although the thermal residual stresses are reduced relative to the non-graded material, their reductions are not so significant in these two systems in comparison with the system without the substrates.

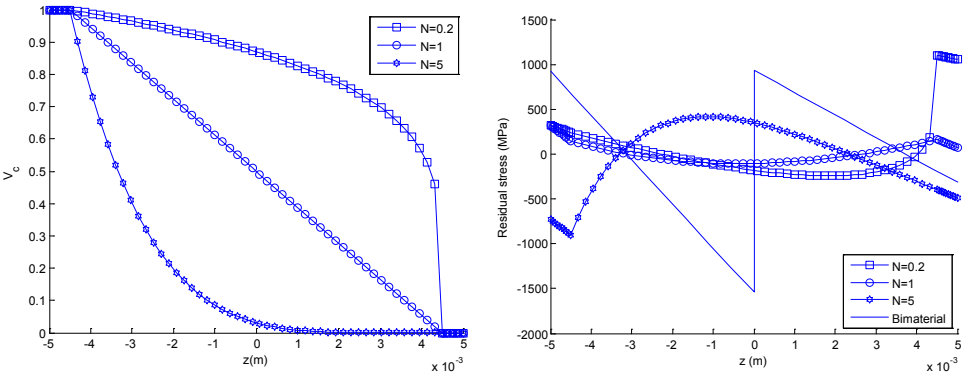

(a) (b)

Figure 5: Volume fraction distribution (a) and thermal residual stresses (b) in the FGM system with substrates of 5% total thickness.

It is obvious that the stresses distribution is pronouncedly influenced by the exponents and thicknesses of the substrates. The results convince that optimal exponents and thicknesses of the substrates would help reduce the maximal thermal residual stresses of a FGM system.

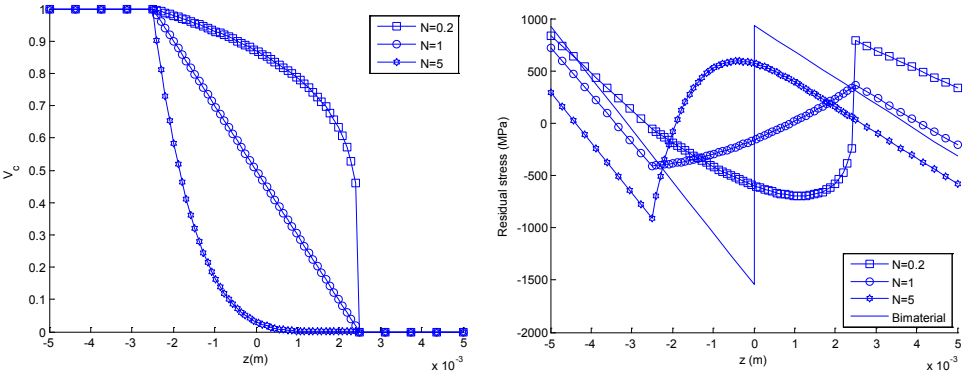

(a) (b)

Figure 6: Volume fraction distribution (a) and thermal residual stresses (b) in the FGM system with substrates of 25% total thicknessb.

4.2 Optimization of exponent

In light of the results in the previous case, a better microstructure of the FGM systems might help minimize thermal residual stresses and enhance its structural reliability in practical applications. In this section, we consider the optimization of the volume fraction distribution to minimize the thermal residual stress of Ni/Al_2O_3 FGM system with different sizes of substrates (0%, 5%, and 25% of the total thickness). The optimal exponent is sought by the GA-PS procedure. The optimization problem is stated as

$$\begin{array}{ll} \text{Find} & N \\ \text{Minimize} & f(N) = \max(\sigma_{t\max}^{FGM}/\sigma_{t\max}^{bi}, \sigma_{c\max}^{FGM}/\sigma_{c\max}^{bi}) \\ \text{Subject to } 0.01 & \leq N \leq 100 \end{array} \tag{12}$$

where $\sigma_{t\max}^{FGM}$ and $\sigma_{c\max}^{FGM}$ are the maximal tensile and compressive residual stresses in the FGM systems.

Tab. 2 presents the optimal results yielded by the GA and GA-PS. Fig. 7 displays volume fractions and thermal residual stresses varying along the thicknesses. The optimization process by the GA and PS for the FGM with different sizes of the substrates (no, 5%, 25%) are displayed in Fig. 8–Fig. 13.

As seen in Tab. 2, three optimal FGM systems with different sizes of the graded region reaches a reduction more than 50% of maximal thermal residual stresses. The optimal system without substrates produces minimal thermal residual stresses. As the thickness of the substrate increases, lager residual stresses are observed in the FGM system.

Table 2: Optimal results for the FGM systems.

Substrates	GA			GA-PS		
Percents	N	$\sigma_{t\max}^{FGM}/\sigma_{t\max}^{bi}$	$\sigma_{c\max}^{FGM}/\sigma_{c\max}^{bi}$	N	$\sigma_{t\max}^{FGM}/\sigma_{t\max}^{bi}$	$\sigma_{c\max}^{FGM}/\sigma_{c\max}^{bi}$
no	1.4200	0.0536	0.0529	1.4210	0.0532	0.0532
5%	1.6134	0.1437	0.1423	1.6160	0.1428	0.1428
25%	2.8412	0.4879	0.4875	2.8435	0.4877	0.4877

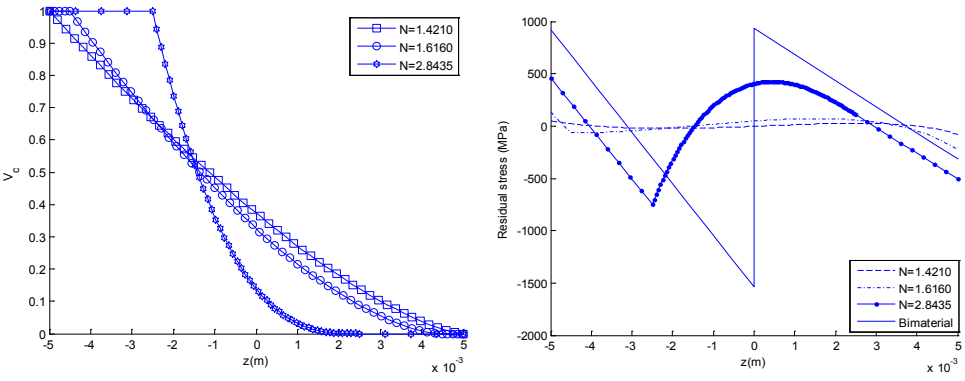

(a) (b)

Figure 7: Volume variation (a) and thermal residual stress distribution (b) for the optimal FGM systems.

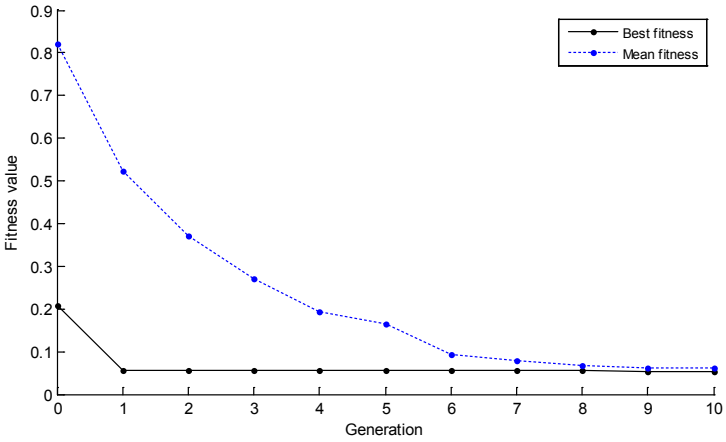

Figure 8: Convergence curves of GA for optimization of the FGM system without substrates.

An assessment of the GA and GA-PS is tabulated in Tab. 2. The GA-PS exhibits better results than the GA in all simulations. The GA quickly locates the promising

region, and obtains the GA solution (Fig. 8, Fig. 10 and Fig. 12). The PS refines the results in the neighborhood of the GA solutions (Fig. 9, Fig. 11 and Fig. 13), despite the fact that the difference between the GA-PS and GA solutions is very small in this case. It is worthnoting that in the GA-PS solutions, $\sigma_{t\max}^{FGM}/\sigma_{t\max}^{bi}$ is much closer to $\sigma_{c\max}^{FGM}/\sigma_{c\max}^{bi}$.

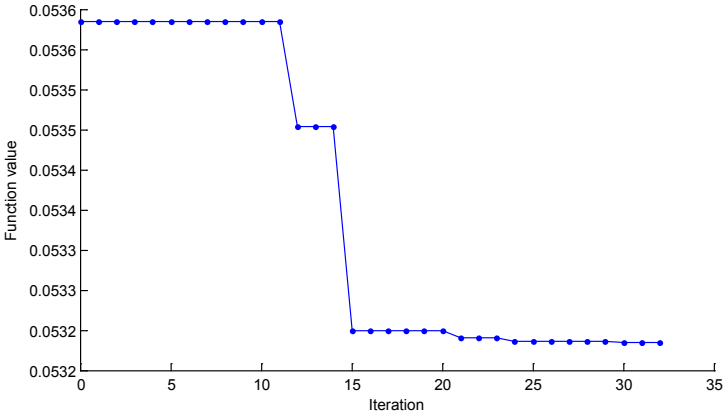

Figure 9: Fine-tuning curves of PS for optimization of the FGM system without substrates.

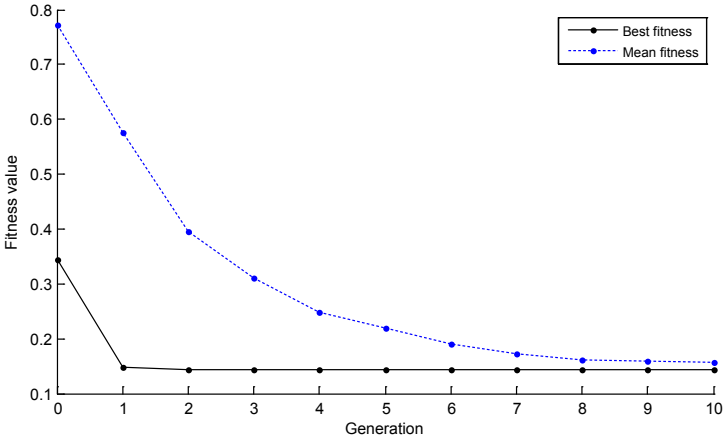

Figure 10: Convergence curves of GA for optimization of the FGM system with substrates of 5% total thickness.

4.3 Optimization of exponent and thickness of substrates

In the previous case, the thermal residual stresses are minimized with controlling the exponent. On the other hand, the thicknesses of the substrates also influence

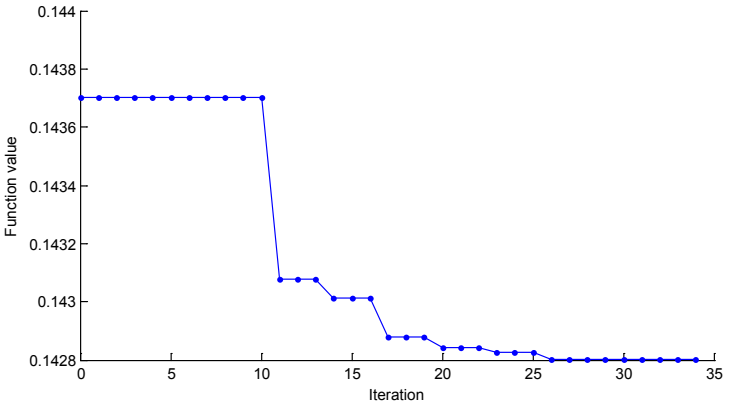

Figure 11: Fine-tuning curves of PS for optimization of the FGM system with substrates of 5% total thickness.

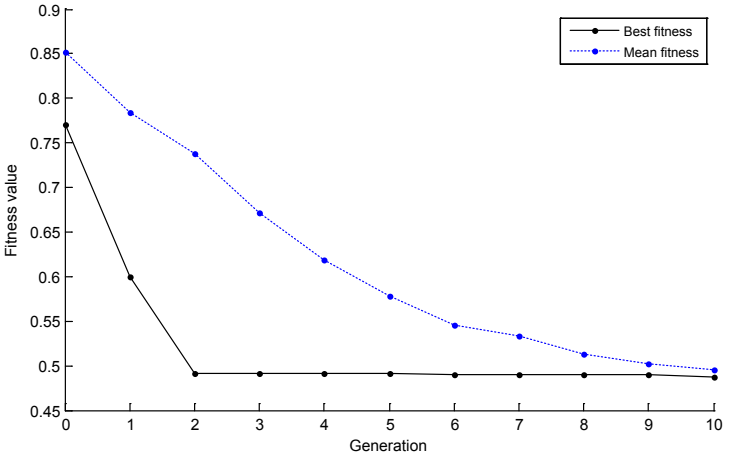

Figure 12: Convergence curves of GA for optimization of the FGM system with substrates of 25% total thickness.

the determination of the thermal residual stresses in the FGMs. In this case, we simultaneously optimize the exponent and thicknesses of the substrates. The optimization problem is:

$$\begin{array}{ll} \text{Find} & N, t_c, t_m \\ \text{Minimize} & f(N,t_c,t_m) = \max(\sigma_{t\max}^{FGM}/\sigma_{t\max}^{bi}, \sigma_{c\max}^{FGM}/\sigma_{c\max}^{bi}) \\ \text{Subject to} & 0.01 \le N \le 100 \\ & 0.001 \le t_c \le 0.0025 \\ & 0.001 \le t_m \le 0.0025 \end{array} \tag{13}$$

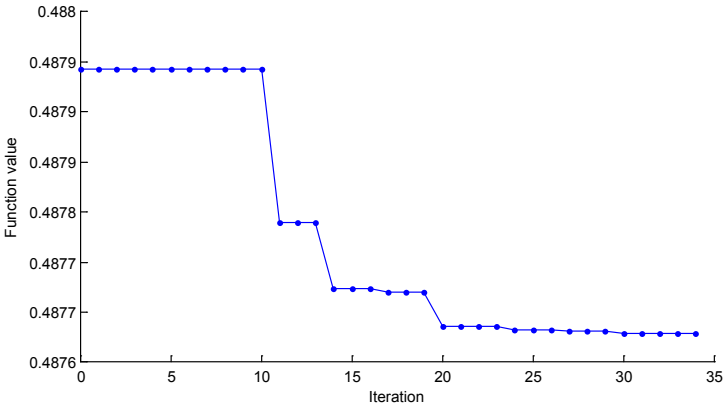

Figure 13: Fine-tuning curves of PS for optimization of the FGM system with substrates of 25% total thickness.

where $\sigma_{t\max}^{FGM}$ and $\sigma_{c\max}^{FGM}$ are the maximal tensile and compressive stresses in the FGM system, t_c and t_m are the thickness of the ceramic and metal substrates. The problem is solved by the GA-PS.

The optimal thicknesses of the ceramic and metal substrates t_c, t_m are respectively 0.00101 m and 0.00118 m, and the optimal exponent is 1.8260. The corresponding stresses ratios, $\sigma_{t\max}^{FGM}/\sigma_{t\max}^{bi}$ and $\sigma_{c\max}^{FGM}/\sigma_{c\max}^{bi}$, are 0.2222 and 0.2229 respectively. That is, nearly 78% reduction of the maximal thermal residual stresses is achieved. The volume fraction and thermal residual stresses along the thickness direction are displayed in Fig. 14.

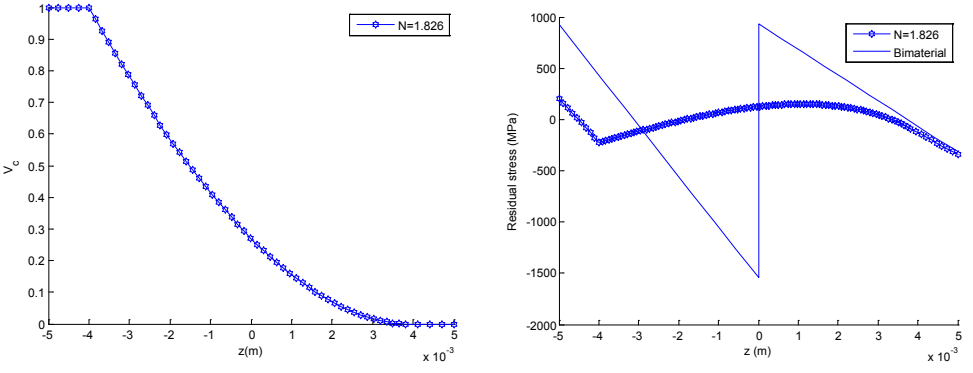

(a) (b)

Figure 14: Volume variation (a) and thermal residual stress distribution (b) for the optimized FGM systems.

4.4 Multi-objective optimization

This section performs a multi-objective optimization problem of the volume fraction distribution. The purpose of the optimization is to tailor the volume fraction distribution and thicknesses of the substrates to simultaneously minimize the mass and the maximal stresses of the FGM system. The optimization is executed with the GA-PS. The multi-objective optimization problem is expressed as:

$$
\begin{aligned}
&\text{Find} && N, t_c, t_m \\
&\text{Minimize} && f(N,t_c,t_m) = \sum_{i=1}^{2} \omega_i f_i(N,t_c,t_m) \\
& && f_1(N,t_c,t_m) = \max(\sigma_{t\max}^{FGM}/\sigma_{t\max}^{bi}, \sigma_{c\max}^{FGM}/\sigma_{c\max}^{bi}) \\
& && f_2(N,t_c,t_m) = \frac{\int [\rho_c V_c + \rho_m (1-V_c)]\, dz - m_{\min}}{m_{\max} - m_{\min}} \\
&\text{Subject to} && 0.01 \le N \le 100 \\
& && 0.001 \le t_c \le 0.0025 \\
& && 0.001 \le t_m \le 0.0025 \\
& && \sigma_{t\max}^{FGM} < \gamma \sigma_{t\max}^{bi} \\
& && \sigma_{c\max}^{FGM} < \gamma \sigma_{c\max}^{bi}
\end{aligned}
\tag{14}
$$

In Eq. (14), $\sigma_{t\max}^{FGM}$ and $\sigma_{c\max}^{FGM}$ are the maximal tensile and compressive stresses in the FGM system, γ is a factor selected as 0.8 to guarantee the maximal tensile and compressive residual stresses smaller than those in the non-graded bimaterial. ρ_c and ρ_m are the densities of the ceramic and metal. m denotes the mass of the FGM along the thickness direction. $m_{\min}$ and $m_{\max}$ are derived when the graded region is pure metal or ceramic. $m_{\max}$ and $m_{\min}$ are respectively 83.88 kg/m^2 and 44.52 kg/m^2. ω_1 is the weight of the first objective function.

Table 3: Results for the GA-PS optimization.

ω_1	N	t_c(e-3)	t_m(e-3)	$\sigma_{t\max}^{FGM}/\sigma_{t\max}^{bi}$	$\sigma_{c\max}^{FGM}/\sigma_{c\max}^{bi}$	$f_1(N)$	$f_2(N)$	$f(N)$
0	0.4127	2.416	1.001	0.7988	0.2208	0.7988	0.2406	0.2406
0.1	0.4182	2.500	1.000	0.7980	0.2220	0.7980	0.2396	0.2954
0.2	0.4202	2.485	1.002	0.7944	0.2216	0.7944	0.2411	0.3518
0.3	0.5163	2.494	1.006	0.6888	0.2102	0.6888	0.2774	0.4008
0.4	0.5539	1.002	1.004	0.5550	0.1679	0.5550	0.3567	0.4360
0.5	1.8444	1.014	1.128	0.2220	0.2219	0.2220	0.6529	0.4375
0.6	1.8515	1.014	1.106	0.2215	0.2215	0.2215	0.6528	0.3940
0.7	1.9035	1.039	1.015	0.2223	0.2223	0.2223	0.6530	0.3515
0.8	1.8374	1.000	1.111	0.2200	0.2200	0.2200	0.6525	0.3065
0.9	1.8231	1.003	1.166	0.2216	0.2215	0.2216	0.6528	0.2647
1.0	1.8691	1.000	1.010	0.2177	0.2178	0.2178	0.6519	0.2178

The optimization results are tabulated in Tab. 3. When ω_1 is smaller than 0.3, the results indicate the weights reduction is dominant in the optimization. Therefore, t_c is near 2.5e-3 and t_m is near 1.0e-3. This is for the reason that the thicker ceramic layer and thinner metal layer lead to a lighter FGM system. While ω_1 is lager than 0.4, both t_m and t_c are near 1.0e-3. In this situation, the thermal residual stresses reduction is more important in the design.

For further analysis, we fix both t_m and t_c at 1.0e-3, and recast the problem (14) as:

$$\begin{aligned}
&\text{Find} && N \\
&\text{Minimize} && f(N) = \sum_{i=1}^{2} \omega_i f_i(N) \\
& && f_1(N) = \max(\sigma_{t\max}^{FGM}/\sigma_{t\max}^{bi}, \sigma_{c\max}^{FGM}/\sigma_{c\max}^{bi}) \\
& && f_2(N) = \frac{\int [\rho_c V_c + \rho_m (1 - V_c)]\, dz - m_{\min}}{m_{\max} - m_{\min}} \\
&\text{Subject to} && 0.01 \le N \le 100 \\
& && \sigma_{t\max}^{FGM} < \gamma \sigma_{t\max}^{bi} \\
& && \sigma_{c\max}^{FGM} < \gamma \sigma_{c\max}^{bi}
\end{aligned} \tag{15}$$

Table 4: Results for the GA-PS optimization.

ω_1	N	$\sigma_{t\max}^{FGM}/\sigma_{t\max}^{bi}$	$\sigma_{c\max}^{FGM}/\sigma_{c\max}^{bi}$	$f_1(N)$	$f_2(N)$	$f(N)$
0	0.3581	0.8000	0.2090	0.8000	0.2637	0.2637
0.2	0.3581	0.8000	0.2090	0.8000	0.2637	0.3709
0.275	0.3581	0.8000	0.2090	0.8000	0.2637	0.4112
0.276	0.4601	0.6648	0.1871	0.6648	0.3151	0.4116
0.277	0.5242	0.5894	0.1735	0.5894	0.3439	0.4119
0.2775	0.5486	0.5624	0.1684	0.5624	0.3543	0.4120
0.278	0.5588	0.5515	0.1663	0.5515	0.3585	0.4121
0.28	0.5588	0.5515	0.1663	0.5515	0.3585	0.4125
0.3	0.5588	0.5515	0.1663	0.5515	0.3585	0.4164
0.4	0.5588	0.5514	0.1663	0.5514	0.3585	0.4357
0.45	0.5588	0.5514	0.1663	0.5514	0.3585	0.4454
0.465	0.5588	0.5514	0.1663	0.5514	0.3585	0.4482
0.4675	1.8721	0.2175	0.2175	0.2175	0.6518	0.4488
0.47	1.8721	0.2175	0.2175	0.2175	0.6518	0.4477
0.5	1.8721	0.2175	0.2175	0.2175	0.6518	0.4347
0.7	1.8721	0.2175	0.2175	0.2175	0.6518	0.3478
1.0	1.8721	0.2175	0.2175	0.2175	0.6518	0.2175

In Fig. 15–Fig. 17, the optimal results with varying weights, ω_1, are displayed.

Some data are selected to be tabulated in Tab. 4. In Fig. 15, we can see the optimized objective function is a continuous piecewise function in terms of the weights ω_1. The value of the optimized objective function is divided into 4 sub-curves with intervals [0, 0.275], [0.275, 0.278], [0.278, 0.4675], [0.4675, 1.0]. In Fig. 16, the curve of the optimal exponent, N, is a discontinuous piecewise function with the same intervals as the optimized objective function. The values of the single objective functions, $\sigma_{t\max}^{FGM}/\sigma_{t\max}^{bi}$, $\sigma_{c\max}^{FGM}/\sigma_{c\max}^{bi}$ and f_2, are plotted in Fig. 17.

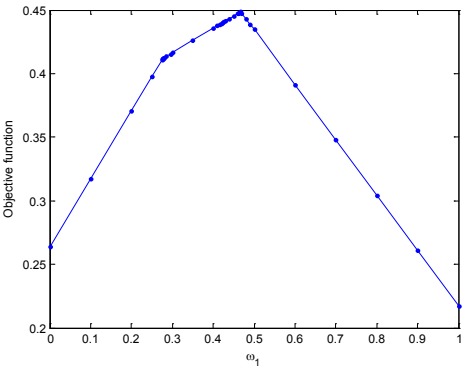

Figure 15: The minimization values of multi-objective function with respect to different weights ω_1.

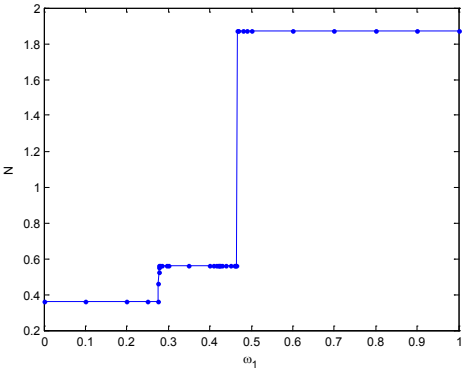

Figure 16: The optimal exponents with respect to different weights ω_1.

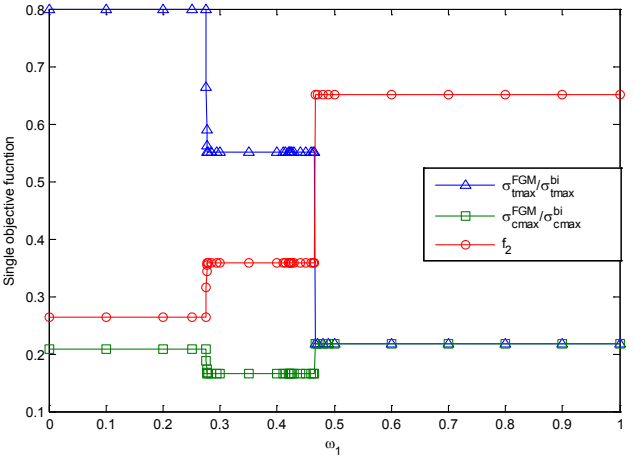

Figure 17: The values of single objective functions with respect to different weights ω_1.

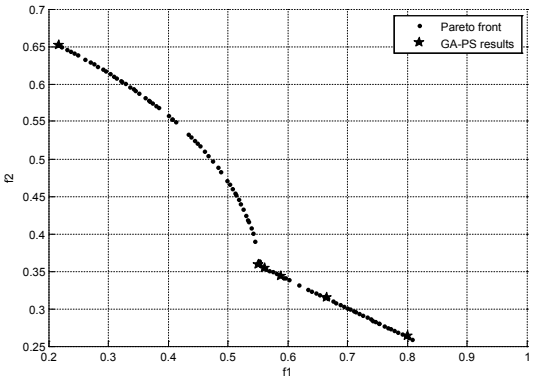

Figure 18: Pareto-optimal front and GA-PS optimization results.

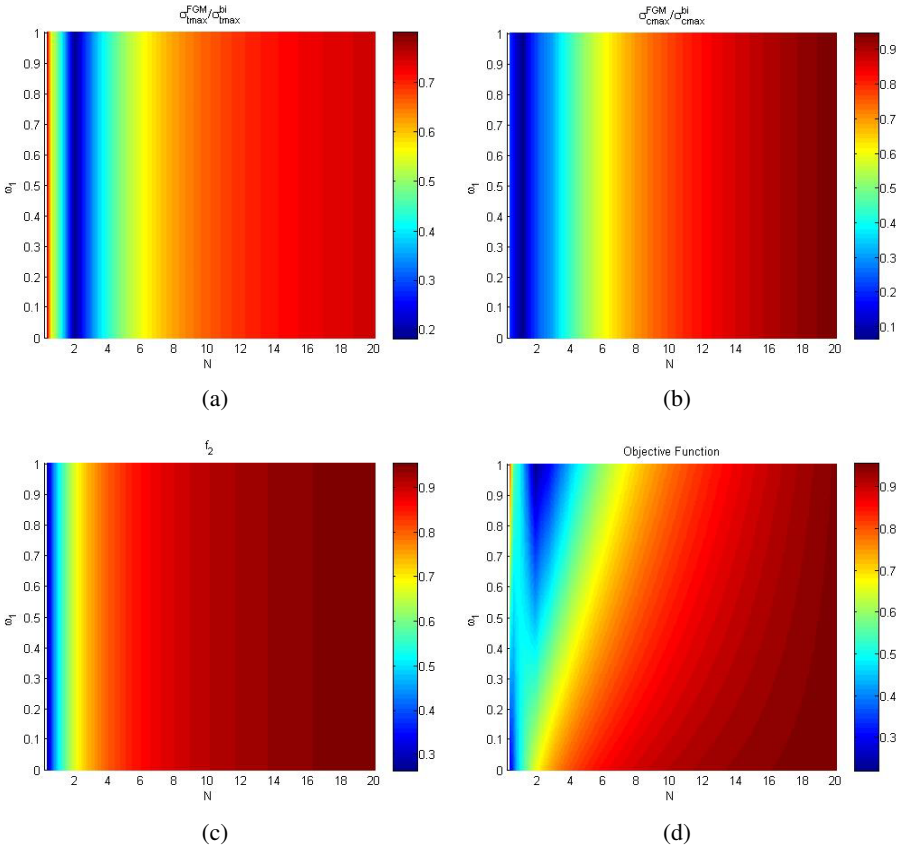

(a) (b)

(c) (d)

Figure 19: (a) Tensile stress ratio; (b) Compressive stress ratio; (c) Value of the second single objective function; (d) Value of the unified objective function.

This result is very similar with the results for problem (14) when $\omega_1 > 0.4$, which confirms the conclusion that the key factor on weight reduction lies in the thickness of the ceramic layer.

Usually, the Pareto-optimal front is employed to seek the group of the non-dominated solutions within the entire feasibility search space. The final Pareto-optimal front of this problem obtained by the multi-objective GA is shown in Fig. 18. It can be observed that the optimization results of the GA-PS almost lie on the Pareto-optimal front.

Furthermore, we depict the figures of the objective functions in terms of weights, ω_1 and exponents, N, as in Fig. 19. It is obvious that our optimization results are in coincidence with these data.

5 Conclusion

The thermal residual stress stemming from cooling down processing temperature plays a significant role in industrial applications of the FGM. In this study, an optimal design for minimizing the thermal residual stresses is presented. The thermal residual stresses are evaluated via an analytical model, in which a hybrid genetic algorithm with the pattern search (GA-PS) is used to search the optima. The promising region is identified by the GA, and the PS is significantly more efficient than the GA in determining local optima. Thus, the number of fitness evolutions is reduced. For a multi-objctive case, the objective functions are normalized and combined with the weighted sum method. The weights are proportional to the relative importance of the objective functions determined by the decision-maker.

From the foregoing numerical experiments, we observe that under the given processing environment, there are mainly two factors affacting the distribution of the thermal residual stresses, *viz* the volume fraction distribution in the graded region and thicknesses of the substrates. The former is assumed as a power law function (P-FGM) in this study and is optimized by seeking an optimal exponent. In an optimal FGM system without substrates, a reduction of almost 95% is achieved in maximal thermal residual stresses. In the optimal FGM systems with substrates of 5% and 25% of total thickness, the maximal residual stress relexation are around 85% and 51%, respectively. On the other hand, as the substrates become thicker, the maximal thermal residual stresses increase. Therefore, the thicknesses of the substrates are always close to the low bound in the constrains in the thermal reduction problems. The thicker ceramic layer would help to reduce the weight of the FGM system.

In conclusion, the proposed methodology is effective to fulfill the capability of the FGM plates in minimizing the maximal thermal residual stresses under different

situations.

Acknowledgement: This work was supported by National Science Funds for Distinguished Young Scholars (Grant No. 11125208) and program of Introducing Talents of Discipline to Universities (111 project, Grant No. B12032).

References

Attia, M.; Meguid, S.; Nouraei, H. (2012): Nonlinear finite element analysis of the crush behaviour of functionally graded foam-filled columns. *Finite Elements in Analysis and Design*, vol. 61, pp. 50–59.

Audet, C.; Dennis, J. (2002): Analysis of Generalized Pattern Searches. *SIAM Journal on Optimization*, vol. 13, pp. 889–903.

Becker Jr, T. L.; Cannon, R. M.; Ritchie, R. O. (2000): An approximate method for residual stress calculation in functionally graded materials. *Mechanics of Materials*, vol. 32, pp. 85–97.

Bouchafa, A.; Benzair, A.; Tounsi, A.; Draiche, K.; Mechab, I.; Adda Bedia, E. A. (2010): Analytical modelling of thermal residual stresses in exponential functionally graded material system. *Materials & Design*, vol. 31, pp. 560–563.

Chen, F.; Jie, W. (2007): Finite element design of MgO/Ni system functionally graded materials. *Journal of Materials Processing Technology*, vol. 182, pp. 181–184.

Cho, J.; Ha, D. (2001): Averaging and finite-element discretization approaches in the numerical analysis of functionally graded materials. *Materials Science and Engineering: A*, vol. 302, pp. 187–196.

Cho, J. R.; Ha, D. Y. (2002): Volume fraction optimization for minimizing thermal stress in Ni-Al_2O_3 functionally graded materials. *Materials Science and Engineering: A*, vol. 334, pp. 147–155.

Deb, K. (2001): Multi objective optimization using evolutionary algorithms: John Wiley and Sons.

Delfosse, D.; Cherradi, N.; Ilschner, B. (1997): Numerical and experimental determination of residual stresses in graded materials. *Composites Part B: Engineering*, vol. 28, pp. 127–141.

Dong, L.; El-Gizawy, A. S.; Juhany, K. A.; Atluri, S. N. (2014): A simple locking-alleviated 4-node mixed-collocation finite element with over-integration, for homogeneous or functionally-graded or thick-section laminated composite beams. *CMC: Computers, Materials & Continua*, vol. 40, pp. 49–77.

Dong, L.; El-Gizawy, A. S.; Juhany, K. A.; Atluri, S. N. (2014): A Simple Locking-Alleviated 3D 8-Node Mixed-Collocation C 0 Finite Element with Over-Integration, for Functionally-Graded and Laminated Thick-Section Plates and Shells, with & without Z-Pins. *CMC: Computers, Materials & Continua*, vol. 41, pp. 163–192.

Elishakoff, I. (2012): Buckling of a column made of functionally graded material. *Archive of Applied Mechanics*, vol. 82, pp. 1355–1360.

Fukui, Y.; Watanabe, Y. (1996): Analysis of thermal residual stress in a thick-walled ring of duralcan-base Al-SiC functionally graded material. *Metallurgical and Materials Transactions A*, vol. 27, pp. 4145–4151.

Goupee, A. J.; Vel, S. S. (2007): Multi-objective optimization of functionally graded materials with temperature-dependent material properties. *Materials & Design*, vol. 28, pp. 1861–1879.

Goupee, A.; Vel, S. (2006): Optimi zation of natural frequencies of bidirectional functionally graded beams. *Structural and Multidisciplinary Optimization*, vol. 32, pp. 473–484.

Hedia, H. S.; Mahmoud, N.-A. (2004): Design optimization of functionally graded dental implant. *Bio-Medical Materials and Engineering*, vol. 14, pp. 133–143.

Koizumi, M. (1997): FGM activities in Japan. *Composites Part B: Engineering*, vol. 28, pp. 1–4.

Lee, W. Y.; Stinton, D. P.; Berndt, C. C.; Erdogan, F.; Lee, Y. D.; Mutasim, Z. (1996): Concept of functionally graded materials for advanced thermal barrier coating applications. *Journal of the American Ceramic Society*, vol. 79, pp. 3003–3012.

Lin, D.; Li, Q.; Li, W.; Zhou, S.; Swain, M. V. (2009): Design optimization of functionally graded dental implant for bone remodeling. *Composites Part B: Engineering*, vol. 40, pp. 668–675.

Markworth, A. J.; Saunders, J. H. (1995): A model of structure optimization for a functionally graded material. *Materials Letters*, vol. 22, pp. 103–107.

Marler, R. T.; Arora, J. S. (2004): Survey of multi-objective optimization methods for engineering. *Structural and Multidisciplinary Optimization*, vol. 26, pp. 369–395.

Nemat-Alla, M. (2003): Reduction of thermal stresses by developing two-dimensional functionally graded materials. *International Journal of Solids and Structures*, vol 40, pp. 7339–7356.

Qian, G.; Nakamura, T.; Berndt, C. C. (1998): Effects of thermal gradient and residual stresses on thermal barrier coating fracture. *Mechanics of Materials*, vol. 27, pp. 91–110.

Ravichandran, K. S. (1994): Elastic Properties of Two-Phase Composites. *Journal of the American Ceramic Society*, vol. 77, pp. 1178–1184.

Ravichandran, K. S. (1995): Thermal residual stresses in a functionally graded material system. *Materials Science and Engineering: A*, vol. 201, pp. 269–276.

Reddy, J. N. (2000): Analysis of functionally graded plates. *International journal for numerical methods in engineering*, vol. 47, pp. 663–684.

Sahay, S. S.; Ravichandran, K. S. (1996): Assessment of residual stresses in a functionally graded material system. *Advanced Composite Newsletter*, vol. 5, no. 4, pp. 1–7.

Shaw, L. L. (1998): Thermal residual stresses in plates and coatings composed of multi-layered and functionally graded materials. *Composites Part B: Engineering*, vol. 29, pp. 199–210.

Srinivas, M.; Patnaik, L. M. (1994): Adaptive probabilities of crossover and mutation in genetic algorithms. *Systems, Man and Cybernetics, IEEE Transactions on*, vol. 24, pp. 656–667.

Taheri, A. H.; Hassani, B.; Moghaddam, N. Z. (2014): Thermo-elastic optimization of material distribution of functionally graded structures by an isogeometrical approach. *International Journal of Solids and Structures*, vol. 51, pp. 416–429.

Tanaka, K.; Watanabe, H.; Sugano, Y.; Poterasu, V. F. (1996): A multicriterial material tailoring of a hollow cylinder in functionally gradient materials: Scheme to global reduction of thermoelastic stresses. *Computer Methods in Applied Mechanics and Engineering*, vol. 135, pp. 369–680.

Wang, H.; Qin, Q.-H. (2008): Meshless approach for thermo-mechanical analysis of functionally graded materials. *Engineering Analysis with Boundary Elements*, vol. 32, pp. 704–712.

Yoshihiro Ootao, Y. T. O. I. (2000): Optimization of material composition of functionally graded plate for thermal stress relaxation using a genetic algorithm. *Journal of Thermal Stresses*, vol. 23, pp. 257–271.

Zhang, X. C.; Xu, B. S.; Wang, H. D.; Jiang, Y.; Wu, Y. X. (2006): Modeling of thermal residual stresses in multilayer coatings with graded properties and compositions. *Thin Solid Films*, vol. 497, pp. 223–231.